

Spontaneous μ - τ Reflection Symmetry Breaking in Neutrino Phenomenology

 Guo-Yuan Huang ¹ , Zhi-Zhong Xing ^{1,2}  and Jing-Yu Zhu ^{1,*} 
¹ Institute of High Energy Physics, School of Physical Sciences, University of Chinese Academy of Sciences, Beijing 100049, China; huanggy@ihep.ac.cn (G.-Y.H.); xingzz@ihep.ac.cn (Z.-Z.X.)

² Center for High Energy Physics, Peking University, Beijing 100080, China

* Correspondence: zhujingyu@ihep.ac.cn; Tel.: +86-132-6155-3785

Received: 15 November 2018; Accepted: 30 November 2018; Published: 4 December 2018



Abstract: The latest global analysis of neutrino oscillation data indicates that the normal neutrino mass ordering is favored over the inverted one at the 3σ level. The best-fit values of the largest neutrino mixing angle θ_{23} and the Dirac CP-violating phase δ are located in the higher octant and the third quadrant, respectively. We show that these experimental trends can be naturally explained by the μ - τ reflection symmetry breaking, triggered by the one-loop renormalization-group equations (RGEs) running from a superhigh energy scale down to the electroweak scale in the framework of the minimal supersymmetric standard model (MSSM). The complete parameter space is numerically explored for both the Majorana and Dirac cases, by allowing the smallest neutrino mass m_1 and the MSSM parameter $\tan\beta$ to vary within their reasonable ranges.

Keywords: lepton flavor mixing; μ - τ reflection symmetry; renormalization group equations

1. Introduction

In the last twenty years, we have witnessed compelling evidence of the neutrino oscillation phenomena [1], as recognized by both the 2015 Nobel Prize in Physics and the 2016 Breakthrough Prize in Fundamental Physics. The standard model (SM) of particle physics must be extended to explain the neutrino masses and the large lepton flavor mixing effects. One can describe the mixings between the three known neutrinos (ν_e, ν_μ, ν_τ) and their mass eigenstates (ν_1, ν_2, ν_3) in terms of a 3×3 unitary matrix, the Pontecorvo–Maki–Nakagawa–Sakata (PMNS) matrix [2,3]:

$$U = P_l \begin{pmatrix} c_{12}c_{13} & s_{12}c_{13} & s_{13}e^{-i\delta} \\ -s_{12}c_{23} - c_{12}s_{13}s_{23}e^{i\delta} & c_{12}c_{23} - s_{12}s_{13}s_{23}e^{i\delta} & c_{13}s_{23} \\ s_{12}s_{23} - c_{12}s_{13}c_{23}e^{i\delta} & -c_{12}s_{23} - s_{12}s_{13}c_{23}e^{i\delta} & c_{13}c_{23} \end{pmatrix} P_\nu, \quad (1)$$

where $c_{ij} \equiv \cos\theta_{ij}$ and $s_{ij} \equiv \sin\theta_{ij}$ (for $ij = 12, 13, 23$) with θ_{ij} being the neutrino mixing angles, $P_l = \text{Diag}\{e^{i\phi_e}, e^{i\phi_\mu}, e^{i\phi_\tau}\}$, and $P_\nu = \text{Diag}\{e^{i\rho}, e^{i\sigma}, 1\}$ with $(\phi_e, \phi_\mu, \phi_\tau)$ and (ρ, σ) being three unphysical phases and two Majorana phases, respectively. Different from the quark sector, there are big mixing angles and a potentially large Dirac CP-violating phase in the lepton sector. On the other hand, the masses of the three known neutrinos are found to be finite, but tiny. It is popular to introduce some heavy degrees of freedom (i.e., the seesaw mechanism [4–8]) and certain flavor symmetries at a superhigh energy scale to explain the smallness of neutrino masses and the lepton flavor mixing patterns observed at low energies. In this case, we need to run the renormalization-group equations (RGEs) to bridge the gap between these two scales.

A credible global analysis of experimental data often points to the truth of particle physics [9,10]. The latest global analysis of available neutrino oscillation data indicates that the normal neutrino

mass ordering ($m_1 < m_2 < m_3$) is favored over the inverted one ($m_3 < m_1 < m_2$) at the 3σ level [11], where m_i (for $i = 1, 2, 3$) stand for the neutrino masses. Moreover, the best-fit value of the atmospheric neutrino mixing angle θ_{23} is slightly larger than 45° (i.e., located in the upper octant), and the best-fit value of the Dirac phase δ is somewhat smaller than 270° (i.e., located in the third quadrant). The μ - τ reflection symmetry [12–14], the minimal discrete flavor symmetry responsible for the nearly maximal atmospheric neutrino mixing and potentially maximal CP violation in neutrino oscillations, can naturally lead to $\theta_{23} = 45^\circ$ and $\delta = 270^\circ$. Assuming this symmetry is realized at a superhigh energy scale, such as the seesaw scale $\Lambda_{\mu\tau}$, it can be spontaneously broken at the electroweak scale $\Lambda_{EW} \sim 10^2$ GeV because of the RGE running effect, leading to the deviations of (θ_{23}, δ) from $(45^\circ, 270^\circ)$. Whether such quantum corrections agree with the experimental results of θ_{23} and δ at low energies depends on the neutrino mass ordering and the theoretical framework accommodating the RGEs [15–22]. We show that the normal neutrino mass ordering, the upper-octant of θ_{23} , and the third-quadrant of δ can be naturally correlated via the RGE-induced μ - τ reflection symmetry-breaking effect in the minimal supersymmetric standard model (MSSM) framework. Based on more reliable experimental data, we numerically explore the almost complete parameter space in both the Dirac and Majorana cases by allowing the smallest neutrino mass m_1 and the MSSM parameter $\tan \beta$ to vary in their reasonable regions. From the final numerical results, one can tell which part of the parameter space is favored by current neutrino oscillation data and which part is ruled out. We also conclude that the best-fit values of θ_{23} and δ [11] may be explained by the spontaneous μ - τ reflection symmetry breaking. The scenario under consideration will be tested in future neutrino oscillation experiments and help to constrain the values of the smallest neutrino mass m_1 , the MSSM parameter $\tan \beta$, and even the Majorana phases. Therefore, our in-depth analysis is timely, general, and suggestive.

2. Spontaneous μ - τ Reflection Symmetry Breaking

2.1. The Majorana Case

If neutrinos are Majorana particles, the μ - τ reflection symmetry requires the Majorana neutrino mass matrix M_ν to be invariant under charge-conjugation transformations $\nu_{eL} \leftrightarrow \nu_{eR}^c, \nu_{\mu L} \leftrightarrow \nu_{\tau R}^c$, and $\nu_{\tau L} \leftrightarrow \nu_{\mu R}^c$. In other words, the corresponding Majorana mass matrix elements $\langle m \rangle_{\alpha\beta} \equiv \sum_i m_i U_{\alpha i} U_{\beta i}$ (for $\alpha, \beta = e, \mu, \tau$ and i running over 1, 2, 3) must be constrained by $\langle m \rangle_{ee} = \langle m \rangle_{ee}^*, \langle m \rangle_{e\mu} = \langle m \rangle_{e\tau}^*, \langle m \rangle_{\mu\mu} = \langle m \rangle_{\tau\tau}^*$ and $\langle m \rangle_{\mu\tau} = \langle m \rangle_{\mu\tau}^*$ [14]. Taking the parametrization form of U as in Equation (1), one immediately obtains the constraints on U as follows: $\theta_{23} = 45^\circ, \delta = 90^\circ$ or $270^\circ, \rho = 0^\circ$ or 90° , and $\sigma = 0^\circ$ or 90° , for the four physical parameters, as well as $\phi_e = 90^\circ$ and $\phi_\mu + \phi_\tau = 0^\circ$ for the three unphysical phases. In the framework of the MSSM, the evolution of M_ν from $\Lambda_{\mu\tau}$ down to Λ_{EW} through the one-loop RGE can be expressed as: [23,24]

$$M_\nu(\Lambda_{EW}) = I_0^2 \left[T_l \cdot M_\nu(\Lambda_{\mu\tau}) \cdot T_l \right] \tag{2}$$

with $T_l = \text{Diag}\{I_e, I_\mu, I_\tau\}$, in which:

$$I_0 = \exp \left[+ \frac{1}{16\pi^2} \int_0^{\ln(\Lambda_{\mu\tau}/\Lambda_{EW})} \left(\frac{3}{5}g_1^2(\chi) + 3g_2^2(\chi) - 3y_t^2(\chi) \right) d\chi \right],$$

$$I_\alpha = \exp \left[- \frac{1}{16\pi^2} \int_0^{\ln(\Lambda_{\mu\tau}/\Lambda_{EW})} y_\alpha^2(\chi) d\chi \right]. \tag{3}$$

Here, $\chi = \ln(\mu/\Lambda_{\mu\tau})$, with μ being an arbitrary renormalization scale between Λ_{EW} and $\Lambda_{\mu\tau}$, g_1 and g_2 denoting the gauge couplings, and y_t and y_α (for $\alpha = e, \mu, \tau$) standing for the Yukawa coupling

eigenvalues of the top quark and charged leptons, respectively. Because of the smallness of y_e and y_μ , one can safely take the approximation $T_l \simeq \text{Diag}\{1, 1, (1 - \Delta_\tau)\}$ with:

$$\Delta_\tau \equiv 1 - I_\tau \simeq \frac{1}{16\pi^2} \int_0^{\ln(\Lambda_{\mu\tau}/\Lambda_{EW})} y_\tau^2(\chi) d\chi. \tag{4}$$

In Figure 1, we show the two-dimensional maps of Δ_τ (left panel) and I_0 (right panel) with respect to $\Lambda_{\mu\tau}$ and $\tan\beta$. One can see that the value of I_0 does not change too much with different settings of $\Lambda_{\mu\tau}$ and $\tan\beta$. In contrast, Δ_τ can change from 0.001–0.05. Shifting the energy scale $\Lambda_{\mu\tau}$ is equivalent to altering $\tan\beta$ to obtain the same value of Δ_τ . In the numerical calculations, we have fixed the μ - τ symmetry scale $\Lambda_{\mu\tau}$ as 10^{14} GeV, with $\tan\beta$ varying in a decent range, i.e. $\tan\beta \in [10, 50]$. We use $\Delta\theta_{23} \equiv \theta_{23}(\Lambda_{EW}) - \theta_{23}(\Lambda_{\mu\tau})$ and $\Delta\delta \equiv \delta(\Lambda_{EW}) - \delta(\Lambda_{\mu\tau})$ to measure the strengths of the RGE-induced μ - τ reflection symmetry breaking effect that are relevant for oscillation experiments. They can be approximated as:

$$\begin{aligned} \Delta\theta_{23} &\simeq \frac{\Delta_\tau}{2} \left(s_{12}^2 \zeta_{31}^{-\eta_\rho} + c_{12}^2 \zeta_{32}^{-\eta_\sigma} \right), \\ \Delta\delta &\simeq \frac{\Delta_\tau}{2} \left[\frac{c_{12}s_{12}}{s_{13}} \left(\zeta_{32}^{-\eta_\sigma} - \zeta_{31}^{-\eta_\rho} \right) - \frac{s_{13}}{c_{12}s_{12}} \left(c_{12}^4 \zeta_{32}^{-\eta_\sigma} - s_{12}^4 \zeta_{31}^{-\eta_\rho} + \zeta_{21}^{\eta_\rho\eta_\sigma} \right) \right], \end{aligned} \tag{5}$$

in which θ_{12} and θ_{13} take their values at Λ_{EW} , $\eta_\rho \equiv \cos 2\rho = \pm 1$ and $\eta_\sigma \equiv \cos 2\sigma = \pm 1$ denote the possible options of ρ and σ in their μ - τ symmetry limit at $\Lambda_{\mu\tau}$, and the ratios $\zeta_{ij} \equiv (m_i - m_j)/(m_i + m_j)$ are defined with m_i and m_j at Λ_{EW} (for $i, j = 1, 2, 3$). In obtaining Equation (5), the μ - τ reflection symmetry conditions $\theta_{23}(\Lambda_{\mu\tau}) = 45^\circ$ and $\delta(\Lambda_{\mu\tau}) = 270^\circ$ have been applied. The corresponding RGE-induced corrections to the other six flavor parameters ($m_1, m_2, m_3, \theta_{12}, \theta_{13}, \rho$, and σ) have been listed in [22]. Unless otherwise specified, the parameters appearing in the subsequent text and equations are all the quantities at Λ_{EW} .

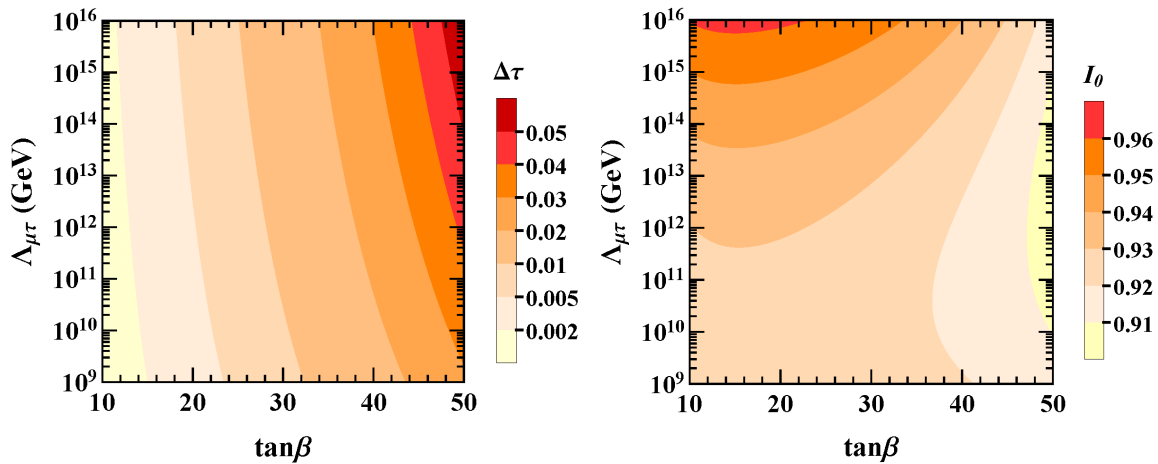


Figure 1. Possible values of Δ_τ (left) and I_0 (right) with respect to $\Lambda_{\mu\tau}$ and $\tan\beta$.

2.2. The Dirac Case

It is also theoretically interesting to combine a pure Dirac mass term M_ν with the μ - τ reflection symmetry for three known neutrinos [20]. In this case, M_ν is invariant under the charge-conjugation transformations $\nu_{eL} \leftrightarrow (\nu_{eL})^c, \nu_{\mu L} \leftrightarrow (\nu_{\tau L})^c$, and $\nu_{\tau L} \leftrightarrow (\nu_{\mu L})^c$ for the left-handed neutrino fields and $N_{eR} \leftrightarrow (N_{eR})^c, N_{\mu R} \leftrightarrow (N_{\tau R})^c$, and $N_{\tau R} \leftrightarrow (N_{\mu R})^c$ for the right-handed neutrino fields. Similar to the Majorana case, this leads to constraints on the mass matrix elements $\langle m \rangle_{\alpha\beta}$ (for $\alpha, \beta = e, \mu, \tau$), i.e., $\langle m \rangle_{ee} = \langle m \rangle_{ee}^*, \langle m \rangle_{e\mu} = \langle m \rangle_{e\tau}^*, \langle m \rangle_{\mu e} = \langle m \rangle_{\tau e}^*, \langle m \rangle_{\mu\tau} = \langle m \rangle_{\tau\mu}^*$, and $\langle m \rangle_{\mu\mu} = \langle m \rangle_{\tau\tau}^*$. Diagonalizing this special mass matrix leads us to the following predictions: $\theta_{23} = 45^\circ, \delta = 90^\circ$ or 270° , and

$2\phi_e - \phi_\mu - \phi_\tau = 180^\circ$ at $\Lambda_{\mu\tau}$. Under the MSSM framework, the one-loop RGE evolution of M_ν from $\Lambda_{\mu\tau}$ to Λ_{EW} can be described as [20]:

$$M_\nu(\Lambda_{EW}) = I_0 \left[T_l \cdot M_\nu(\Lambda_{\mu\tau}) \right], \tag{6}$$

where the definitions of I_0 and T_l are the same as those in Equations (2) and (3). Using the same conventions as in the Majorana case, the deviations of θ_{23} and δ between Λ_{EW} and $\Lambda_{\mu\tau}$ can be expressed as:

$$\begin{aligned} \Delta\theta_{23} &\simeq \frac{\Delta\tau}{4} \left[c_{12}^2 \left(\zeta_{32} + \zeta_{32}^{-1} \right) + s_{12}^2 \left(\zeta_{31} + \zeta_{31}^{-1} \right) \right], \\ \Delta\delta &\simeq \frac{\Delta\tau}{4} \left[\frac{c_{12} \left(s_{12}^2 - c_{12}^2 s_{13}^2 \right)}{s_{12} s_{13}} \left(\zeta_{32} + \zeta_{32}^{-1} \right) - \frac{s_{12} \left(c_{12}^2 - s_{12}^2 s_{13}^2 \right)}{c_{12} s_{13}} \left(\zeta_{31} + \zeta_{31}^{-1} \right) \right. \\ &\quad \left. - \frac{s_{13}}{c_{12} s_{12}} \left(\zeta_{21} + \zeta_{21}^{-1} \right) \right]. \end{aligned} \tag{7}$$

The expressions for deviations of $m_1, m_2, m_3, \theta_{12}, \theta_{13}, \rho$, and σ can be found in [22]. The analytical approximations made in Equations (5) and (7) are instructive and helpful for understanding the RGE-induced μ - τ reflection symmetry-breaking effect. However, the accuracy will be quite poor if the neutrino masses are strongly degenerate. Therefore, we have to use the numerical approach to evaluate the spontaneous μ - τ reflection symmetry-breaking effect and to explore the allowed parameter space by fitting the current experimental data.

3. Numerical Exploration

In the framework of MSSM, we input the constraints of the μ - τ reflection symmetry as initial conditions at $\Lambda_{\mu\tau} \sim 10^{14}$ GeV and numerically run the RGEs from $\Lambda_{\mu\tau}$ down to Λ_{EW} . To be more concrete, the initial conditions include $\theta_{23} = 45^\circ$ and $\delta = 270^\circ$, as well as four different cases of ρ and σ for Majorana neutrinos: Case A: $\rho = \sigma = 0^\circ$; Case B: $\rho = \sigma = 90^\circ$; Case C: $\rho = 0^\circ$ and $\sigma = 90^\circ$; Case D: $\rho = 90^\circ$ and $\sigma = 0^\circ$. For any given values of the MSSM parameter $\tan\beta$ and the smallest neutrino mass m_1 at Λ_{EW} , we scan the other relevant neutrino oscillation parameters like $\{\sin^2\theta_{12}, \sin^2\theta_{13}, \Delta m_{sol}^2, \Delta m_{atm}^2\}$ at $\Lambda_{\mu\tau}$ over properly wide ranges by utilizing the MultiNest program [25–27]. The conventions $\Delta m_{sol}^2 \equiv m_2^2 - m_1^2$ and $\Delta m_{atm}^2 \equiv m_3^2 - (m_1^2 + m_2^2)/2$ have been adopted to keep consistent with the definitions in [11]. For each scan, the neutrino mixing parameters at Λ_{EW} are yielded and then compared with their global-fit values by minimizing:

$$\chi^2 \equiv \sum_i \frac{(\xi_i - \bar{\xi}_i)^2}{\sigma_i^2}. \tag{8}$$

Here, $\xi_i \in \{\sin^2\theta_{12}, \sin^2\theta_{13}, \Delta m_{sol}^2, \Delta m_{atm}^2\}$ stand for the parameters at Λ_{EW} , which are produced by the RGE running from $\Lambda_{\mu\tau}$; $\bar{\xi}_i$'s represent the best-fit values of ξ_i in the global analysis; and σ_i 's are the corresponding symmetrized 1σ errors. We take the best-fit values and the 1σ errors of the six neutrino oscillation parameters in [11]: $\sin^2\theta_{12} = 3.04_{-0.13}^{+0.14} \times 10^{-1}$, $\sin^2\theta_{13} = 2.14_{-0.07}^{+0.09} \times 10^{-2}$, $\sin^2\theta_{23} = 5.51_{-0.70}^{+0.19} \times 10^{-1}$, $\delta = 1.32_{-0.18}^{+0.23} \times \pi$, $\Delta m_{sol}^2 = 7.34_{-0.14}^{+0.17} \times 10^{-5}$ eV², $\Delta m_{atm}^2 = 2.455_{-0.032}^{+0.035} \times 10^{-3}$ eV². The smallest neutrino mass m_1 is allowed to take values over the range $[0, 0.1]$ eV, and the MSSM parameter $\tan\beta$ may vary from 10–50. With this setup, we examine how significantly θ_{23} and δ at Λ_{EW} can deviate from their initial values at $\Lambda_{\mu\tau}$ by incorporating the recent global-fit results [11].

3.1. The Majorana Case

In Figures 2 and 3, we plot the allowed values of θ_{23} and δ at Λ_{EW} by taking different values of m_1 and $\tan\beta$ with $\chi^2 = 0$. Four different cases of the initial Majorana phases (ρ, σ) at $\Lambda_{\mu\tau}$ have

been considered. For each point in the m_1 - $\tan\beta$ plane, θ_{23} and δ are determined simultaneously. The boundary conditions for the RGEs include both the initial values of $\{\theta_{23}, \delta, \rho, \sigma\}$ at $\Lambda_{\mu\tau}$ and the experimental constraints on $\{\sin^2\theta_{12}, \sin^2\theta_{13}, \Delta m_{\text{sol}}^2, \Delta m_{\text{atm}}^2\}$ at Λ_{EW} . In this case, the RGEs may not have a realistic solution for some combinations of m_1 and $\tan\beta$; the gray-gap regions in Figures 2 and 3 (Cases C and D) are excluded. There is no such gap in Cases A and B with different initial values of ρ and σ . The RGE running effect always pushes θ_{23} to the higher octant and, in most cases, leads δ to the third quadrant, just the right direction as indicated by the best-fit values of these two quantities [11]. In Case A and Case D, θ_{23} may be significantly corrected for $m_1 \simeq 0.1$ eV and $\tan\beta \simeq 50$. Of course, such an evolution will be strongly disfavored by the experimental information of θ_{23} , which has not been included for this analysis. Our main purpose is to show the general magnitudes of RGE corrections to θ_{23} and δ , without directly involving the experimental limits on them. In Case B, θ_{23} is not sensitive to the RGE running. The RGE-induced corrections to δ in Cases A and B are very weak. We highlight Case D, in which the best-fit point $(\theta_{23}, \delta) \simeq (48^\circ, 238^\circ)$ is reachable for the same settings of m_1 and $\tan\beta$.

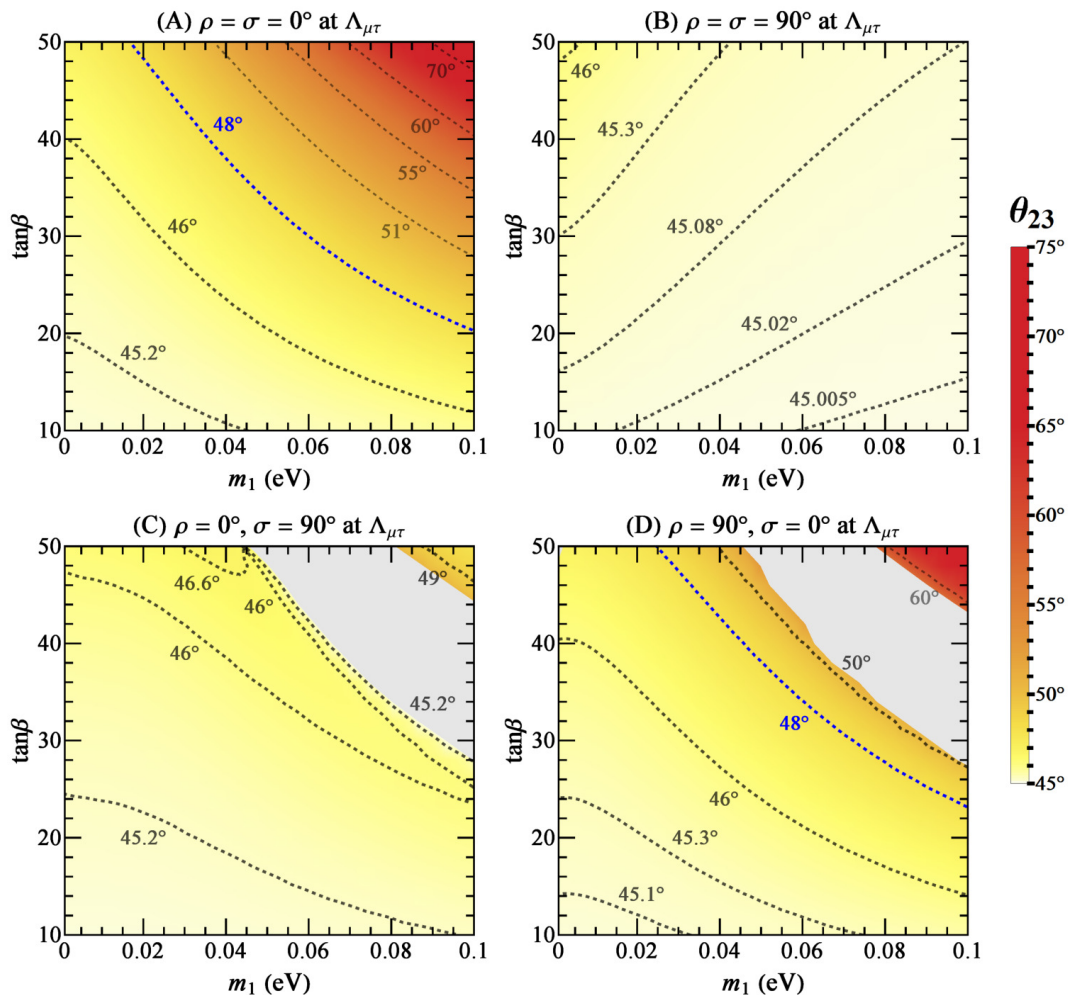


Figure 2. The values of θ_{23} at Λ_{EW} due to the spontaneous μ - τ reflection symmetry-breaking effect, where the dashed curves are the contours with some typical values of θ_{23} and the blue ones agree with the best-fit result of θ_{23} in [11].

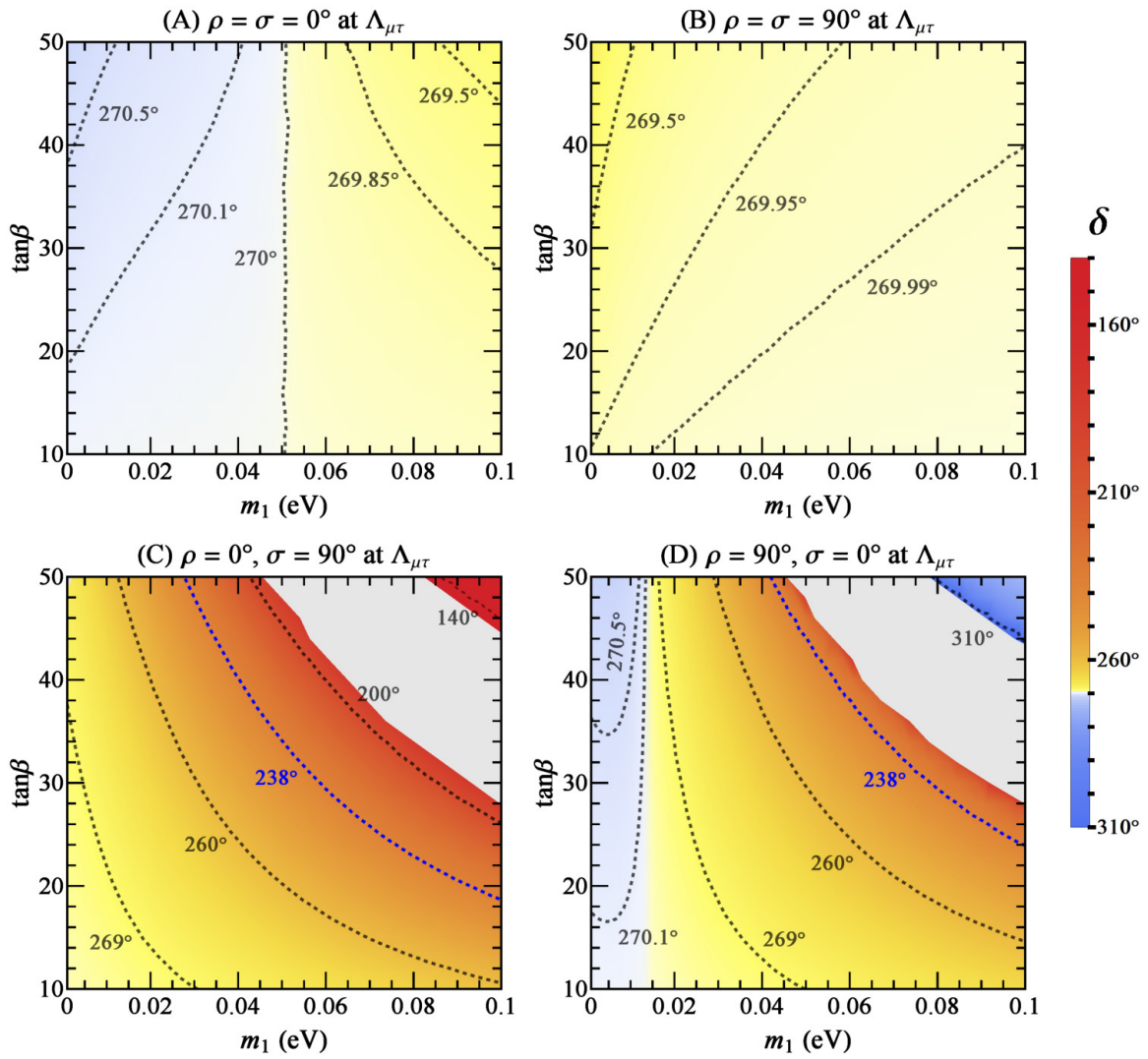


Figure 3. The values of δ at Λ_{EW} due to the spontaneous μ - τ reflection symmetry-breaking effect, where the dashed curves are the contours with some typical values of δ and the blue ones agree with the best-fit result of δ in [11].

The RGE corrections to θ_{23} and δ in Figures 2 and 3 can be understood with the help of the analytical expressions in Equation (5), if the neutrino masses are not so degenerate. The factor Δ_τ is essentially proportional to $\tan^2 \beta$ as a result of $y_\tau^2 \propto (1 + \tan^2 \beta) \simeq \tan^2 \beta$ for $\tan \beta \gtrsim 10$, and the magnitudes of $\Delta\theta_{23}$ and $\Delta\delta$ always increase with $\tan^2 \beta$. Because the factors Δ_τ and $\zeta_{31} \simeq \zeta_{32}$ are all positive for the normal mass ordering, the sign of $\Delta\theta_{23}$ is always positive. The dependence of $\Delta\theta_{23}$ and $\Delta\delta$ on the neutrino mass m_1 is different for the four options of ρ and σ at $\Lambda_{\mu\tau}$. In the region of small m_1 and $\tan \beta$, the radiative correction to θ_{23} is proportional to m_1 for Cases A, C, and D, but it is inversely proportional to m_1 in Case B with $\eta_\rho = \eta_\sigma = -1$. As for $\Delta\delta$, its value depends on two terms: one is enhanced by $1/\sin \theta_{13}$; and the other is suppressed by $\sin \theta_{13}$. However, the latter one can become dominant in some cases. For example, in Case A, the first term $\propto 1/\sin \theta_{13}$ is positive and dominant when the neutrino mass m_1 is relatively small, while the second term $\propto \sin \theta_{13}$ is negative and will gradually dominate when the value of m_1 increases.

To see the correlation between θ_{23} and δ at Λ_{EW} , we marginalize m_1 and $\tan \beta$ over the reasonable ranges $m_1 \in [0, 0.1]$ eV and $\tan \beta \in [10, 50]$ and show the results in Figure 4.

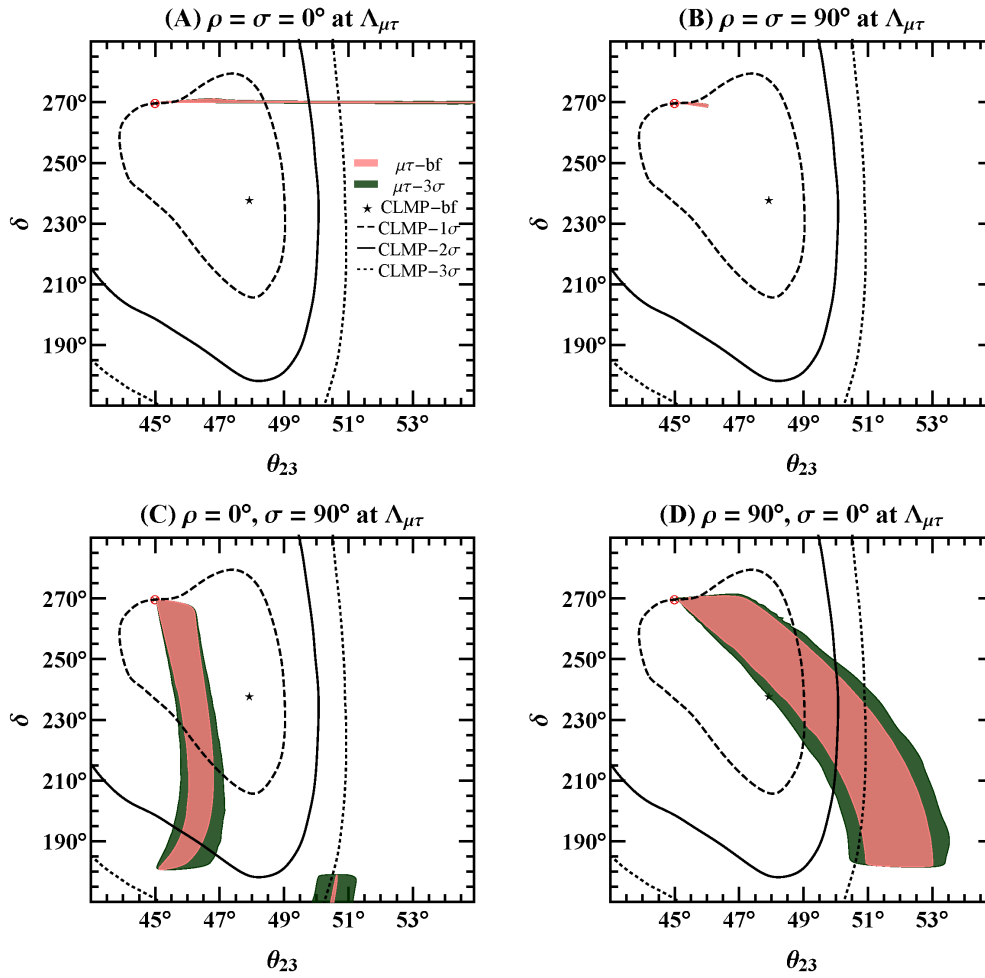


Figure 4. The correlation between θ_{23} and δ at Λ_{EW} compared with the global-fit results (represented with “CLMP”) [11], where m_1 and $\tan\beta$ are marginalized over $[0, 0.1]$ eV and $[10, 50]$, respectively. The red circled cross \otimes signifies the point $(\theta_{23}, \delta) = (45^\circ, 270^\circ)$. The pink regions are allowed for θ_{23} and δ when $\{\sin^2\theta_{12}, \sin^2\theta_{13}, \Delta m_{sol}^2, \Delta m_{atm}^2\}$ at Λ_{EW} all take their best-fit values. The green region is allowed when these four observables are relaxed from their best-fit values to their 3σ ranges.

The recent global-fit results [11] are given as the black contours for the 1σ (dashed), 2σ (solid), and 3σ (dotted) confidence levels. The best-fit point of the global analysis is marked as the black star. We notice that the μ - τ reflection symmetry point $(\theta_{23}, \delta) = (45^\circ, 270^\circ)$ at Λ_{EW} , which is marked as the red circled cross in the plot, is on the dashed contour. This means that $\theta_{23}(\Lambda_{EW}) = 45^\circ$ and $\delta(\Lambda_{EW}) = 270^\circ$ are statistically disfavored at the 1σ level [11]. For the pink regions, the best-fit values of $\{\sin^2\theta_{12}, \sin^2\theta_{13}, \Delta m_{sol}^2, \Delta m_{atm}^2\}$ can be simultaneously reached (i.e., $\chi_{\min}^2 = 0$). If the value of χ_{\min}^2 is relaxed to 11.83 (i.e., the 3σ confidence level for two degrees of freedom), the wider green regions of θ_{23} and δ will be allowed. In the two upper panels of Figure 4, which correspond to Cases A (left one) and B (right one), the allowed range of δ is very narrow; this feature is compatible with the two upper panels of Figure 3 where δ varies less than 1° . In these two cases, the green region almost overlaps with the pink region. In the two lower panels of Figure 4, corresponding to Cases C (left one) and D (right one), the RGE-induced corrections of θ_{23} and δ are both significant. The separate shaded region around $\theta_{23} \simeq 50^\circ$ in Figure 4C is associated with the small upper-right corner of the parameter space in Figure 2C or Figure 3C. There is a similar separate shaded region in Case D, but it is outside the chosen ranges of θ_{23} and δ in plotting Figure 4D, and its confidence level is much weaker, outside the 3σ region in the global analysis.

3.2. The Dirac Case

The corresponding numerical analysis for the Dirac neutrinos is much easier due to the absence of two Majorana phases. Similar to the Majorana case, the allowed regions of θ_{23} and δ at Λ_{EW} and their intimate correlation are illustrated in Figures 5 and 6. The analytical approximations of $\Delta\theta_{23}$ and $\Delta\delta$ in Equation (7) can be further simplified to:

$$\begin{aligned} \Delta\theta_{23} &\simeq \frac{\Delta_\tau}{2} \frac{m_2^2 + m_3^2}{\Delta m_{atm}^2}, \\ \Delta\delta &\simeq -\frac{\Delta_\tau}{2} \frac{s_{13}}{c_{12}s_{12}} \frac{m_1^2 + m_2^2}{\Delta m_{sol}^2}. \end{aligned} \tag{9}$$

It is easy to see that bigger values of m_1 and $\tan\beta$ lead to larger deviations of (θ_{23}, δ) from $(45^\circ, 270^\circ)$. In particular, θ_{23} and δ are always located in the upper octant and the third quadrant, respectively. In Figure 5, we have the gray regions for the same reason as that in the Majorana case. Similar to Case D in the Majorana case, the spontaneous μ - τ reflection symmetry breaking can take (θ_{23}, δ) very close to their best-fit point in the global analysis.

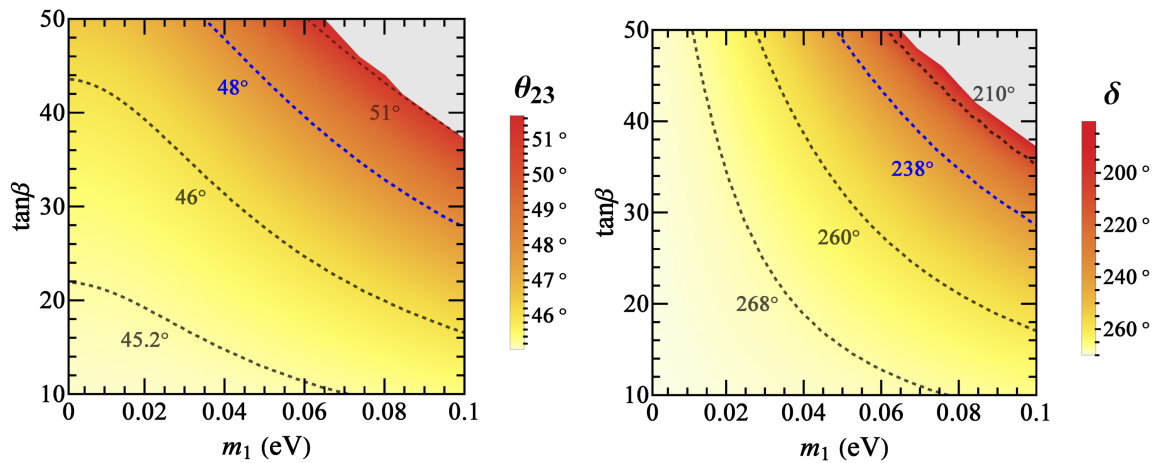


Figure 5. For the Dirac case, the allowed values of θ_{23} (left) panel and δ (right) panel at Λ_{EW} are owed to the spontaneous μ - τ reflection symmetry-breaking effect. The dashed curves are the contours with some typical values of θ_{23} and δ , and the blue ones stand for the best-fit result of θ_{23} or δ in [11].

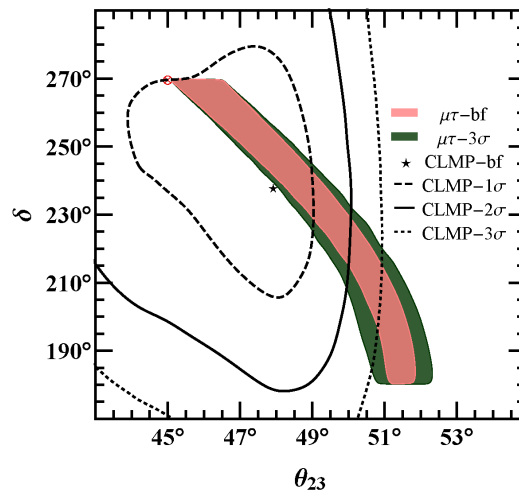


Figure 6. The correlation of (θ_{23}, δ) at Λ_{EW} for the Dirac case. The conventions are the same as Figure 4.

4. Conclusions

The μ - τ reflection symmetry is inclusive to explain the nearly maximal atmospheric neutrino mixing and the potentially maximal CP violation in neutrino oscillations. However, the latest global analysis suggests this symmetry should be broken at the low energy experimental scale. The RGE running effect can be responsible for the symmetry breaking. The normal neutrino mass ordering, the upper-octant of θ_{23} , and the third-quadrant of δ can be naturally correlated with the RGEs running effect in the MSSM framework. Some of our main observations are subject to the chosen theoretical framework, i.e., the MSSM. The reasons why we do not consider the standard model is: (a) in the SM, the RGE running effect is always very small; (b) in the SM, the running direction of θ_{23} from $\Lambda_{\mu\tau}$ down to Λ_{EW} is opposite its current best-fit result in the normal mass ordering case; and (c) there may be the vacuum-stability problem as the energy scale is above 10^{10} GeV [28,29] in the SM. On the other hand, the best-fit values of θ_{23} and δ will unavoidably fluctuate in the future when more experimental data are accumulated and included in the global analysis. Since we have generally explored the complete parameter space, our results still keep working. If the future precision measurements favor the inverted neutrino mass ordering, the lower octant of θ_{23} , and (or) another quadrant of δ , one can perform the numerical analysis in the same way, either within or beyond the MSSM. In the same spirit, one may study other interesting flavor symmetries and their RGE-induced breaking effect, in order to link model building at high-energy scales effectively with the observed neutrino oscillation data at low energies.

Author Contributions: All authors contributed equally to this paper.

Funding: This research work was supported in part by the National Natural Science Foundation of China under Grant No. 11775231 and Grant No. 11775232.

Acknowledgments: We would like to thank the organizers of the 7th International Conference on New Frontiers in Physics (ICNFP 2018), where this work was reported.

Conflicts of Interest: The authors declare no conflict of interest.

References

1. Tanabashi, M. Particle Data Group. Review of Particle Physics. *Phys. Rev. D* **2018**, *98*, 030001.
2. Maki, Z.; Nakagawa, M.; Sakata, S. Remarks on the unified model of elementary particles. *Prog. Theor. Phys.* **1962**, *28*, 870–880.
3. Pontecorvo, B. Neutrino Experiments and the Problem of Conservation of Leptonic Charge. *Sov. Phys. JETP* **1968**, *26*, 984–988.
4. Minkowski, P. $\mu \rightarrow e\gamma$ at a Rate of One Out of 10^9 Muon Decays? *Phys. Lett. B* **1977**, *67*, 421–428. [[CrossRef](#)]
5. Yanagida, T. Horizontal Symmetry And Masses Of Neutrinos. In Proceedings of the Workshop on the Unified Theories and the Baryon Number in the Universe, Tsukuba, Japan, 13–14 February 1979; Sawada, O., Sugamoto, A., Eds.; National Laboratory for High Energy Physics: Tsukuba, Japan, 1979; p. 95.
6. Gell-Mann, M.; Ramond, P.; Slansky, R. Complex Spinors and Unified Theories. In *Supergravity*; van Nieuwenhuizen, P., Freedman, D., Eds.; North Holland Publishing Co.: Amsterdam, The Netherlands, 1979; p. 315.
7. Glashow, S.L. The Future of Elementary Particle Physics. In *Quarks and Leptons*; Lévy, M., Basdevant, J.L., Speiser, D., Weyers, J., Gastmans, R., Jacob, M., Eds.; Springer: Boston, MA, USA, 1980; p. 687.
8. Mohapatra, R.N.; Senjanovic, G. Neutrino Mass and Spontaneous Parity Violation. *Phys. Rev. Lett.* **1980**, *44*, 912.
9. Fogli, G.L.; Lisi, E.; Marrone, A.; Palazzo, A.; Rotunno, A.M. Hints of $\theta_{13} > 0$ from global neutrino data analysis. *Phys. Rev. Lett.* **2008**, *101*, 141801. [[CrossRef](#)] [[PubMed](#)]
10. An, F.P.; Bai, J.Z.; Balantekin, A.B.; Band, H.R.; Beavis, D.; Beriguete, W.; Bishai, M.; Blyth, S.; Boddy, K.; Brown, R.L.; et al. Observation of electron-antineutrino disappearance at Daya Bay. *Phys. Rev. Lett.* **2012**, *108*, 171803. [[PubMed](#)]
11. Capozzi, F.; Lisi, E.; Marrone, A.; Palazzo, A. Current unknowns in the three neutrino framework. *Prog. Part. Nucl. Phys.* **2018**, *102*, 48–72.

12. Babu, K.S.; Ma, E.; Valle, J.W.F. Underlying A(4) symmetry for the neutrino mass matrix and the quark mixing matrix. *Phys. Lett. B* **2003**, *552*, 207–213. [[CrossRef](#)]
13. Harrison, P. F.; Scott, W. G. μ - τ reflection symmetry in lepton mixing and neutrino oscillations. *Phys. Lett. B* **2002**, *547*, 219–228. [[CrossRef](#)]
14. Xing, Z.Z.; Zhao, Z.H. A review of μ - τ flavor symmetry in neutrino physics. *Rept. Prog. Phys.* **2016**, *79*, 076201. [[CrossRef](#)] [[PubMed](#)]
15. Luo, S.; Xing, Z.Z. Resolving the octant of θ_{23} via radiative μ - τ symmetry breaking. *Phys. Rev. D* **2014**, *90*, 073005.
16. Zhou, Y.L. μ - τ reflection symmetry and radiative corrections. *arXiv* **2014**, arXiv:1409.8600.
17. Zhao, Z.H. Breakings of the neutrino μ - τ reflection symmetry. *J. High Energy Phys.* **2017**, *2017*, 023. [[CrossRef](#)]
18. Rodejohann, W.; Xu, X.J. Trimaximal μ - τ reflection symmetry. *Phys. Rev. D* **2017**, *96*, 055039.
19. Liu, Z.C.; Yue, C.X.; Zhao, Z.H. Neutrino μ - τ reflection symmetry and its breaking in the minimal seesaw. *J. High Energy Phys.* **2017**, *2017*, 102.
20. Xing, Z.Z.; Zhang, D.; Zhu, J.Y. The μ - τ reflection symmetry of Dirac neutrinos and its breaking effect via quantum corrections. *J. High Energy Phys.* **2017**, *2017*, 135.
21. Nath, N.; Xing, Z.Z.; Zhang, J. μ - τ Reflection Symmetry Embedded in Minimal Seesaw. *Eur. Phys. J. C* **2018**, *78*, 289. [[CrossRef](#)]
22. Huang, G.Y.; Xing, Z.Z.; Zhu, J.Y. Correlation of normal neutrino mass ordering with upper octant of θ_{23} and third quadrant of δ via spontaneous μ - τ symmetry breaking. *arXiv* **2018**, arXiv:1806.06640.
23. Ellis, J.R.; Lola, S. Can neutrinos be degenerate in mass? *Phys. Lett. B* **1999**, *458*, 310. [[CrossRef](#)]
24. Fritzsch, H.; Xing, Z.Z. Mass and flavor mixing schemes of quarks and leptons. *Prog. Part. Nucl. Phys.* **2000**, *45*, 1–81. [[CrossRef](#)]
25. Feroz, F.; Hobson, M.P. Multimodal nested sampling: An efficient and robust alternative to MCMC methods for astronomical data analysis. *Mon. Not. R. Astron. Soc.* **2008**, *384*, 449–463. [[CrossRef](#)]
26. Feroz, F.; Hobson, M.P.; Bridges, M. MultiNest: An efficient and robust Bayesian inference tool for cosmology and particle physics. *Mon. Not. R. Astron. Soc.* **2009**, *398*, 1601–1614. [[CrossRef](#)]
27. Feroz, F.; Hobson, M.P.; Cameron, E.; Pettitt, A.N. Importance Nested Sampling and the MultiNest Algorithm. *arXiv* **2013**, arXiv:1306.2144.
28. Xing, Z.Z.; Zhang, H.; Zhou, S. Impacts of the Higgs mass on vacuum stability, running fermion masses and two-body Higgs decays. *Phys. Rev. D* **2012**, *86*, 013013.
29. Elias-Miro, J.; Espinosa, J.R.; Giudice, G.F.; Isidori, G.; Riotto, A.; Strumia, A. Higgs mass implications on the stability of the electroweak vacuum. *Phys. Lett. B* **2012**, *709*, 222–228.



© 2018 by the authors. Licensee MDPI, Basel, Switzerland. This article is an open access article distributed under the terms and conditions of the Creative Commons Attribution (CC BY) license (<http://creativecommons.org/licenses/by/4.0/>).